Ankle Joint Intrinsic Dynamics is More Complex than a Mass-Spring-Damper Model

Ehsan Sobhani Tehrani, *Member, IEEE*, Kian Jalaleddini, *Member, IEEE*, and Robert E. Kearney, *Life Fellow, IEEE*

***Abstract*— This paper describes a new small signal parametric model of ankle joint intrinsic mechanics in normal subjects. We found that intrinsic ankle mechanics is a third-order system and the second-order mass-spring-damper model, referred to as IBK, used by many researchers in the literature cannot adequately represent ankle dynamics at all frequencies in a number of important tasks. This was demonstrated using experimental data from five healthy subjects with no voluntary muscle contraction and at seven ankle positions covering the range of motion. We showed that the difference between the new third-order model and the conventional IBK model increased from dorsi to plantarflexed position. The new model was obtained using a multi-step identification procedure applied to experimental input/output data of the ankle joint. The procedure first identifies a non-parametric model of intrinsic joint stiffness where ankle position is the input and torque is the output. Then, in several steps, the model is converted into a continuous-time transfer function of ankle compliance, which is the inverse of stiffness. Finally, we showed that the third-order model is indeed structurally consistent with agonist–antagonist musculoskeletal structure of human ankle, which is not the case for the IBK model.**

***Index Terms*— Ankle joint biomechanics, dynamic stiffness, system identification, intrinsic stiffness, ankle dynamic compliance, muscle tendon complex (MTC), non-parametric models, parametric system dynamics.**

I. Introduction

ANKLE joint dynamics describe the dynamic relationship between joint position and the torque acting about it. It is represented and studied in the literature in three different but related forms: a) *stiffness* with position as input and torque as output [1]; b) *impedance* with differential change in ankle position as input and torque as output [2]; and c) *compliance*, the inverse of stiffness, with torque as the input and position as output [3]. Regardless of the form, ankle dynamics has two main components [1]: i) *Intrinsic* due to the passive viscoelastic and inertial properties of the limb, joint and connective tissue in addition to the active properties of contracting muscle fibers; and ii) *Reflex* originating from stretch reflex induced changes in muscle activation. Both components play critical roles in human movement since they define the properties of the musculoskeletal load that the central nervous system must control.

Modeling the *intrinsic* component of ankle mechanics has been extensively studied in the literature in both active [4], [5] and relaxed muscle conditions [6], [7]. The identified models can be broadly classified into two groups: *static* where the ankle behavior is treated as an instantaneous function of position and can be represented as an elastic element; and *dynamic* where the behavior is a function of the position history and/or its derivatives .

Static models have been used and estimated in various ways that can be grouped into three categories: **i)** The slope of the joint torque-angle curve during large movements with no fast perturbations [4], [6], [8], [9], which is often called quasi-stiffness. In most of these studies, the authors deliberately used very slow ramp-and-hold input perturbations to maintain the ankle in quasi-static conditions where dynamic contributions are small. Rouse *et al.* [10] state that quasi-stiffness is equivalent to static stiffness in passive joints but distinct from it in powered joints. **ii)** The short-range stiffness defined as the ratio between changes in joint torque and small changes in joint position [11]–[14]. This is sometimes called "perturbation induced" stiffness because the definition implies a perturbation-like change in joint position. Nonetheless, it should be regarded as a static model since it does not capture the transient responses or dynamics of the joint. **iii)** The stiffness matrix, often represented by ellipsoids, for modeling static stiffness in more than 1 degrees of freedom (e.g. [15], [16]). Such models may predict ankle behavior in response to low-frequency perturbations or the steady-state response to small amplitude step perturbations but cannot model the response to position changes with wider frequency content observed during function.

Dynamic joint models can be divided into two main groups: **i)** Non-parametric impulse response function (IRF) or frequency response models (e.g. [4], [6], [17]–[21], [22]); and **ii)** Second-order mechanical models with inertia (I), viscous (B), and elastic (K) terms. This IBK model has been used to study a wide variety of joints in quasi-stationary

Manuscript received December 9, 2015; revised June 21, 2016 and December 16, 2016; accepted February 9, 2017. Date of publication March 8, 2017; date of current version September 2, 2017. This work was supported by the NPRP from the Qatar National Research Fund (a member of Qatar Foundation) under Grant 6-463-2-189. The statements made herein are solely the responsibility of the authors.

E. Sobhani Tehrani and R. E. Kearney are with the Department of Biomedical Engineering, McGill University, Montréal, QC H3A 2B4, Canada (e-mail: ehsan.sobhani@mail.mcgill.ca; robert.kearney@mcgill.ca).

K. Jalaleddini is with the Division of Biokinesiology and Physical Therapy, University of Southern California, Los Angeles, CA 90033 USA (e-mail: seyed.jalaleddini@mail.mcgill.ca).

Digital Object Identifier 10.1109/TNSRE.2017.2679722

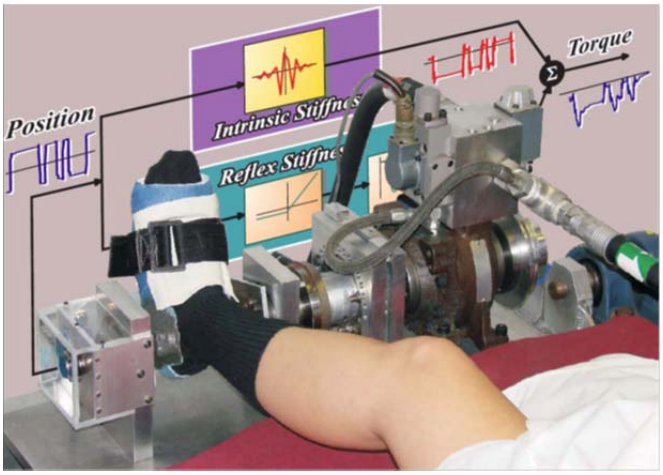

Fig. 1. The experimental apparatus used for perturbing the ankle and measuring joinr position and torque to identify dynamic stiffness.

conditions (e.g. ankle [5], [7], [23], knee [24], wrist [13]). The model has also been used to study stiffness during time-varying conditions (e.g. ankle [2], [22], [25], knee [26], elbow [27], the end-point of the upper arm [28], [29]). Finally, inverse IBK model was used in [30] to represent knee joint compliance (i.e., inverse of stiffness). Most of these studies have reported that the IBK models predict the output very well. However, we recently observed that under some conditions a non-parametric IRF model predicted the output more accurately than the IBK model. Examination of the torque prediction residuals of the IBK model showed evidence of unmodelled dynamics that were not present in the residuals of the IRF. This deviation from second-order IBK behaviour was also observed in previous work (Lee *et al.* [4]), which led us to investigate systematically the nature of the deviations from IBK model and the dependence of these deviations on ankle position. Specifically, we have tried to answer four important research questions: 1) What the IBK model fails to represent? 2) Why we see deviations from IBK and at what ankle positions these deviations are larger? 3) What is the nature of the non-parametric IRF model that outperforms the IBK? Note that the IRF model itself provides very little insight into the system's characteristics. 4) Is there a physiologically relevant explanation or physiological consistency for the deviations observed?

This paper presents the results of these investigations, which demonstrates that under passive conditions ankle intrinsic mechanics are more accurately modelled by a third-order model than the conventional second-order IBK model. Moreover, we showed that the third-order model is structurally consistent with the agonist-antagonist organization of the ankle muscles.

II. Methods

A. Experiments

We recruited five healthy subjects {S1, S2, S3, S4, S5} , four males and a female, with no history of ankle pathologies. All subjects gave informed consent to the experimental procedures approved by McGill University's institutional review board. Subjects lay supine with their left foot firmly attached to the pedal of an electro-hydraulic actuator using a custom built fiberglass boot and remained relaxed throughout the experiment. The experimental setup is shown in Fig. 1 and described in details in [23].

The actuator was operated as a very stiff position servo. The neutral position (0.0 rad) for all subjects corresponded to a 90° angle between the foot and shank. The Dorsiflexed (DF) positions and torques dorsiflexing the ankle were taken as positive. Consequently, negative values correspond to Plantarflexed (PF) position and plantarflexing torques. Small amplitude *Pseudo Random Arbitrarily Level Distributed Signal* (PRALDS) position perturbations were applied at seven ankle positions, selected in random order, through the range of motion $\{-0.3, -0.2, -0.1, 0.0, +0.05, +0.1, +0.15\}$ radians while subjects remained at rest throughout the experiment. PRALDS is a piecewise constant random signal whose constant levels are selected from a V-shaped distribution with a peak at zero and whose pulse durations have a uniform distribution over a desired range. The peak to peak amplitude of PRALDS was set to 0.07 (i.e., ± 0.035) radians to maintain the joint near each position operating point to minimize nonlinear and time-varying effects. The PRALDS pulse durations were selected from a uniform distribution with minimum of 90 ms and maximum of 110 ms. These relatively short pulse durations were selected to (a) increase mean absolute velocity or zero-crossing rate of the perturbations to suppress reflex response [31] and (b) increase the bandwidth of the perturbations to enable more accurate identification of intrinsic dynamics. We used PRALDS rather than other commonly used PRBS (pseudo random binary sequence) and BLG (band-limited Gaussian) perturbations because for any peak-to-peak amplitude: 1) PRALDS has a power spectral density (PSD) that is flatter than that of PRBS and its total power is much larger than BLG and close to that of PRBS; and 2) The amplitude distribution of PRALDS is more uniform than that of PRBS or BLG. Thus, PRLADS provides the best trade-off between PSD shape, amplitude distribution, and signal power for any signal amplitude.

Each trial lasted 90 s, where ankle angular position in sagittal plane (PF/DF), joint torque, and surface EMGs from *Tibialis Anterior* (TA) and three heads of *Triceps Surae* (TS) muscles; i.e., Soleus, Gastrocnemius Medial (GM) and Lateral (GL) were recorded. Data were recorded at 1 kHz and decimated to 200 Hz for model identification. Surface EMGs were first recorded using single differential electrodes, then were amplified (1000 times), band-pass filtered (20-2000 Hz), digitized, and full-wave rectified. We monitored EMGs to determine if a subject had reflex response during a trial. Specifically, first we searched for EMG spikes with amplitudes larger than twice the standard deviation of the EMG at REST condition. Thus, four of the subjects (S1, S2, S3 and S5) had no reflexes in any trials (i.e., 56 trials: 4 subjects, 7 positions, 2 trials per position). Only 8 trials with subject S4 at few DF positions had some reflex responses. We inspected these visually to determine if they were synchronized with rising edges of the

PRALDS position perturbations (i.e. stretches) with a delay of about 40 ms. If reflex response existed and was stationary, we first used a method developed by Jalaleddini *et al.* [32] to decompose the measured torque into its intrinsic and reflex components and then used the intrinsic torque for modeling the intrinsic mechanics. If reflexes were non-stationary, we did not use the data from those trails. The stationarity of the reflex activity was determined by monitoring the amplitudes of reflex EMG spikes over time. If the amplitudes remained quasi-constant, the reflex was considered stationary. In fact, only two out of 8 trials with reflexes were non-stationary, which were so obvious that they were easily detected by visual inspection.

B. Identification Models and Algorithms

We used three model structures and identification algorithms to relate ankle position to ankle torque: (1) second-order IBK model, (2) Non-parametric discrete-time IRF model, and (3) Parametric continuous-time transfer function (TF) model.

(1) IBK Model: The IBK model relates the measured ankle torque sampled at discrete time step k to ankle position θ_k, velocity $\dot{\theta}_k$, and acceleration $\ddot{\theta}_k$

$$T_k = I_a\ddot{\theta}_k + B_a\dot{\theta}_k + K_a\theta_k \tag{1}$$

where I_a, B_a and K_a are the ankle inertia, viscous, and elastic parameters. $\ddot{\theta}_k$ and $\dot{\theta}_k$ were computed numerically from the position signal recorded at 1 kHz (using a five-point parabolic fit method). We used ordinary least squares to estimate the IBK parameters from input/output data (decimated at 200 Hz).

(2) Non-Parametric IRF Model: The discrete-time IRF model relates ankle position to torque through the discrete convolution sum

$$T_k = t_s \sum_{l=-L}^{+L} h_l \cdot \theta_{k-l} \tag{2}$$

where t_s is the sampling period; θ_{k-l} is the measured ankle position lagged l sample times; and $\{h_l; l = -L, \ldots, 0, \ldots, +L\}$ are the *unknown* two-sided IRF coefficients at lags $l = -L, \ldots, 0, \ldots, +L$. We estimated these coefficients from input/output data (decimated to 200Hz) using a robust IRF identification technique, Westwick and Kearney [19]. The lengths of the intrinsic stiffness IRFs were set to 0.05 s for all subjects since increasing the length did not improve torque prediction accuracy.

(3) Parametric TF Model: The non-parametric IRF model in (2) does not provide the insight into the underlying system that a parametric model would. However, ankle stiffness IRF is two-sided (e.g. [7], [33]) and consequently cannot be represented by a proper (i.e. stable and causal) transfer function or state-space (SS) model. Therefore, the well-known linear parametric identification techniques such as subspace [34] and prediction error minimization (PEM) [35] methods cannot estimate stiffness dynamics directly. Instead, we identified a TF model of *ankle compliance* which was then inverted to obtain stiffness. However, identifying compliance directly with measured torque as input and position as output will yield biased results since any torque noise (measurement noise and baseline voluntary contraction) will appear at the input.

Consequently, we developed a multi-step identification approach to convert the identified stiffness IRF to a continuous-time compliance transfer function. First, we simulated the identified stiffness IRF with the experimental position input to generate a noise-free torque signal. This was then used as the input to identify a discrete-time, SS model of ankle compliance using a subspace approach [36], [37] that estimates both the system order and parameters. The resulting identified SS model was then converted to a discrete-time TF

$$H_c(z) = \frac{\Theta(z)}{\mathrm{T}(z)} = C(zI - A)^{-1}B + D. \tag{3}$$

Then, we converted it to continuous-time using the inverse bi-linear transform

$$H_c(s) = \frac{\Theta(s)}{\mathrm{T}(s)} = H_c(z)|_{z=\frac{2+st_s}{2-st_s}} \tag{4}$$

where A, B, C and D are the estimated discrete-time state-space matrices; z is the forward shift operator of Z-transform; s is the Laplace operator; and $H_c(z)$ and $H_c(s)$ are the discrete-time and continuous-time ankle dynamic compliance transfer functions, respectively.

The above multi-step parametric identification procedure can be summarized as follows:

Step-1: Identify a discrete-time two-sided IRF model of intrinsic stiffness using measured position as input and measured torque as output.

Step-2: Simulate the IRF model with the input position used in Step-1 to generate a *noise-free* version of joint torque.

Step-3: Use subspace identification method [36] with noise-free torque as input and measured position as output to estimate both the model order and discrete-time state-space matrices of ankle dynamic compliance.

Step-4: Convert the discrete-time state-space model to a continuous-time transfer function model of ankle dynamic compliance using (3) and (4).

Step-5: Invert the compliance transfer function to obtain the stiffness model; i.e. $H_s(s) = \frac{\mathrm{T}(s)}{\Theta(s)} = H_c^{-1}(s)$.

C. Model Evaluation Criteria

We used three criteria for comparing the performance of the IBK model with that of the IRF model of ankle stiffness, prior to converting it to a compliance transfer function.

(1) The %VAF of torque prediction by the models

$$\%VAF = 100\left(1 - \frac{var\left(T_k - \hat{T}_k\right)}{var\left(T_k\right)}\right). \tag{5}$$

The VAF was used as a measure of overall predictive ability. Two other criteria were computed to account for model complexities (i.e. number of model parameters):

(2) The minimum description length (MDL) of the model

$$MDL(M) = \left(1 + \frac{Mlog(N)}{N}\right)\sum_{k=1}^{N}\left(T_k - \hat{T}_k\right)^2. \tag{6}$$

(3) The difference between the Akaike Information Criterion (ΔAIC) of the two models

$$\Delta AIC = Nlog\left(\frac{SSE_{irf}}{SSE_{ibk}}\right) + 2\left(M_{irf} - M_{ibk}\right) \qquad (7)$$

where $N = 18000$ is the number of samples for 90-s trials decimated at 200 Hz; M in (6) is the number of parameters of each model, thus $M_{ibk} = 3$ and $M_{irf} = 21$ for the IRFs of all subjects with $t_s = 5ms$; $\hat{T}_k$ is the torque predicted by each model; and SSE_{irf} and SSE_{ibk} are the sum of squared errors [the right most term in (6)] of the IRF and IBK models, respectively. Note that the MDL and AIC are two commonly used model selection metrics that compare the *relative* quality of two or more models identified from a data set. Both metrics deal with a trade-off between the predictive accuracies (or goodness of fit) of the models and their number of parameters. There is a general belief that the MDL tends to favor lower number of parameters over accuracy while AIC tends to favor higher accuracy over number of parameters. Thus, if both metrics select the same model among other candidates, that model can be trusted.

Finally, we used frequency responses (FRs) to compare the identified parametric compliance TF (M_{ctf}) with the IBK and IRF stiffness models. This first required converting the stiffness models into a compliance form. We used a simple inversion for the IBK model ($M_{ibk^{-1}}$). However, for the IRF model, we first simulated it with a white input and then estimated the frequency response of the *compliance IRF* (M_{cirf}) using the simulated output as input and the white input as output. To quantify the difference between the FRs of any two models $M_1, M_2 \in \left\{M_{ibk^{-1}}, M_{cirf}, M_{ctf}\right\}$, we calculated the root mean squared magnitude of error (RMSME) between their complex numbers over a frequency range of $[f_{min}, 50]$ Hz

$$f\text{RMSME}_{M_1,M_2} = \sqrt{\frac{1}{N_f}\sum_{n=1}^{N_f}\left|M_1\left(j\omega_n\right) - M_2\left(j\omega_n\right)\right|^2} \qquad (8)$$

where $f_{min} = f_s/N_{FFT}$ in which $f_s = 200$ Hz is the sampling frequency of the data used for identification and N_{FFT} is the number of FFT points used to calculate the FRs. We used $N_{FFT} = 4000$ in our analysis. Thus, $N_f = \frac{1}{4}N_{FFT} + 1 = 1001$; and $\omega_1 = 2\pi f_{min}$ and $\omega_{N_f} = 2\pi \times 50$ (rad/s).

III. Results

A. Typical Experimental Data

Figure 2 shows data from a typical trial performed at -0.3rad ankle position. Fig. 2A shows ankle position as imposed by the actuator and Fig. 2B is the measured ankle torque (solid blue) and the torque predicted by the identified stiffness IRF model (dashed red). It is evident that the IRF model has predicted ankle torque very well. Ankle position stayed near -0.3 rad and thus the torque was quasi-stationary. Fig. 2C and D show *processed* EMGs of Soleus and TA muscles. It is evident that there is no relation between the EMGs and the position indicating that there were no reflex responses. Also, the subject had very little background activation (corresponding to muscle tone) as he was instructed to remain at rest. This can be observed in Fig. 2C and D where the two EMGs (and their RMS values in black dashed lines) at REST condition are well below their RMS values during PF and DF contractions at 15% Maximum Voluntary Contraction (MVC) (in green dashed dots). We measured the MVC at each ankle position in both the plantarflexion and dorsiflexion directions. Thus, MVC was taken as themaximum of torque in trials of 75 s in which subjects were instructed to exert their maximum voluntary torque on the pedal following a square-wave with period of 15 s and duty cycle of 1/3. Only subject S4 showed reflex response in some of the trials at neutral and DF positions, where we used the decomposition approach [38] to remove the reflex torque from the measured torque. The maximum reflex torque contribution to the total torque was found to be only 10% (VAF).

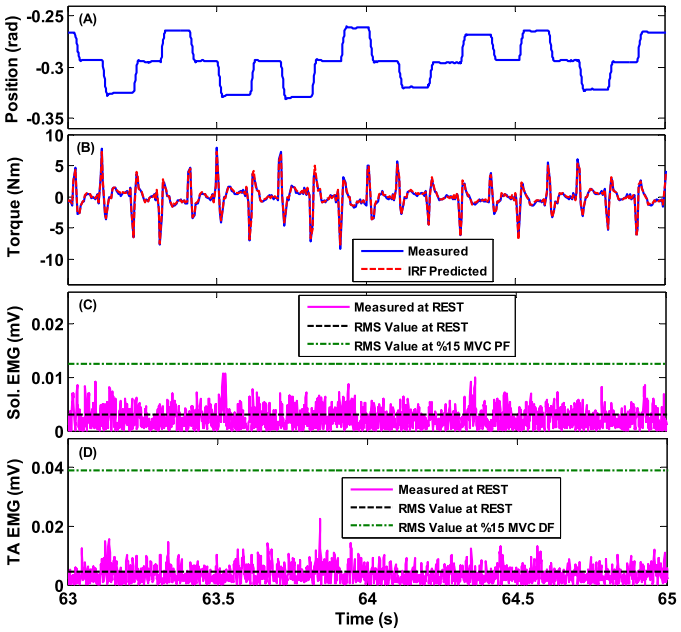

Fig. 2. A 2-second segment of the experimental data from a trial with subject S2 at rest at -0.3rad ankle position: (A) position; (B) measured torque (solid blue) and torque predicted by the IRF model (dashed red); and processed (C) Soleus and (D) TA EMGs. In (C) and (D), the black dashed lines represent the RMS values of the measured EMG signals. The green dash-dots represent the RMS values of the EMG signal in PF and DF contractions with 15% MVC.

B. Comparison of the Stiffness IRF and IBK Models

The dynamics of the identified IRF and IBK models were quite different. We used experimental data of the five subjects at PF position of -0.3 rad to identify IBK and discrete-time IRF models of ankle stiffness. For all subjects, the IRF model represented intrinsic stiffness more accurately than the IBK model: (i) The IRF predicted torque with a larger VAF than the IBK model for all subjects as shown in Table I; (ii) The IBK torque prediction residuals were considerably greater than those of the IRF during the dynamic response to perturbations as shown in Fig. 3A for subject S3; (iii) The PSD of the IRF residuals were clearly smaller than those of the IBK specially

TABLE I
THE %VAF OF THE IDENTIFIED IBK AND IRF MODELS OF INTRINSIC DYNAMIC STIFFNESS IN PREDICTING MEASURED ANKLE TORQUE IN ADDTION TO THE MDL RATIOS AND THE AIC DIFFERENCE BETWEEN THE TWO MODELS AT A PF ANKLE POSITION (−0.3 radians) FOR FIVE SUBJECTS

Subject	S1	S2	S3	S4	S5
IBK %VAF	90.5	87.6	86.3	85.7	92.0
IRF %VAF	97.6	96.3	96.8	96.9	95.8
MDL_{ibk}/MDL_{irf}	3.7	3.2	3.9	4.5	1.8
ΔAIC	-2.3E4	-2.1E4	-2.4E4	-2.7E4	-1.1E4

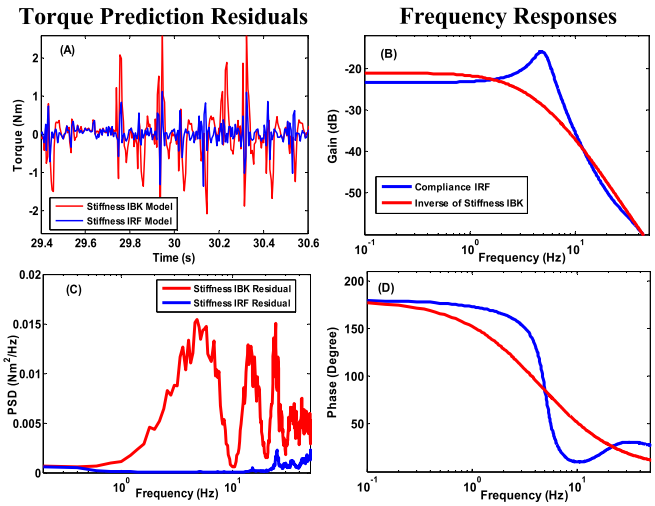

Fig. 3. Torque prediction residuals and frequency responses of the IRF and IBK models of ankle intrinsic mechanics identified at −0.3rad ankle position for subject S3: (A,C) residuals in time domain and their power spectral densities PSD; (B,D) the gain and phase of the frequency responses of the compliance IRF and the inverse of stiffness IBK.

over the frequency range of [0.5,40]Hz as shown in Fig. 3C for subject S3; (iv) the gain (Fig. 3B) and phase (Fig. 3C) of the frequency responses of the compliance IRF and the inverse IBK models were quite different. Similar results were observed for the other four subjects. Note that the observations (ii) to (iv) complement the first observation about VAF in the sense that they highlight the dynamical nature of the difference between the IRF and the IBK model.

We also showed that the improved VAF is not due to IRF having more parameters than the IBK model. Thus, the MDL of the IRF model was at least 3.2 times smaller than the IBK model for the first four subjects and 1.8 times smaller for subject S5 as shown in Table I. In addition, the difference between the AIC of the IBK and IRF models were negative for all subjects as also shown in Table I. These confirm that the additional parameters in the IRF model contribute to describing the true ankle dynamics.

Finally, we suspected that an underdamped IBK model might provide a better fit to the resonance frequency than least squares estimation in the time domain. Fitting the IBK model in the frequency domain did result in a lower damping ratio and better fit to the resonance. However, this fit was worse in the lower frequencies and resulted in 3 to 10% lower torque prediction VAF (see Section A of the Supplementary Material). Thus, we concluded that a second-order model cannot fit both the resonance and low frequencies at the same time due to insufficient degrees of freedom in the second-order model compared to a higher order model.

C. Effect of Ankle Position

The IBK and IRF models depended systematically on ankle position as Fig. 4 illustrates for a typical subject. Thus, (1) The compliance resonance frequency systematically increased from about 5 Hz at −0.3 rad PF to almost 12 Hz at +0.15 rad DF; (2) The low-frequency (or DC) gain of ankle compliance decreased as the joint was dorsiflexed; (3) The difference between the compliance IRF model and the inverse IBK model increased from DF to PF. Similar observations were made in the other four subjects participated in the study. The difference between IBK and IRF models had both static and dynamic components. The static component is evident in the difference between the low-frequency gains. The dynamic component is evident in the differences between the gains at the resonance frequencies and the phases. Moreover, Fig. 4 shows that the PSD of the torque predicted by stiffness IRF much more closely matched that of the measured torque at almost all frequencies compared with the stiffness IBK predicted torque. Specifically, the difference was more significant in the frequency range of [0.5, 15] in PF, [5, 15] Hz in Neutral, and [10, 15] Hz in DF ankle position. The two frequency ranges corresponding to PF and Neutral positions are both relevant to human locomotion and voluntary control, and consistent with (and rather wider than) the frequency range of [5,8] Hz found in prior work (Lee *et al.* [4]).

The phase plots of Fig. 4 further support deviation from second order IBK behaviour. Unlike the IBK models, the phase of the IRF models will *not* converge to 180°. For example, at PF ankle position, the phase of the inverse IBK model at 50 Hz was 12.3° while that of the IRF model was 27.7°. Moreover, the phase *trends* of the two models are distinct and different. The IBK phase starting at 180° *monotonically* decreased with frequency, which is expected from an inverse IBK model with two poles and no zeros. However, the phase of the compliance IRF changes its trend at around 10 Hz (in PF position) and 20 Hz (in Neutral and DF positions) and starts to *increase* with frequency, which is an indication of additional pole-zeros in the system.

Fig. 4 also shows the coherence between measured ankle torque and position perturbations around three ankle positions (PF, Neutral, and DF). Coherence quantifies how much output power is linearly correlated with the input at each frequency. It is evident from Fig. 4 that the coherence was large (>0.9) at all frequencies in all ankle positions *except* (a) at Neutral position where it dropped sharply at 10 Hz and (b) at DF position where it dropped sharply at 5, 10 and 15 Hz. These coherences indicate that a linear model describes joint stiffness extremely well and nonlinear effects either do not exist or are extremely small. We believe that the sharp drops arise because of *tremor* since the spectra of EMGs

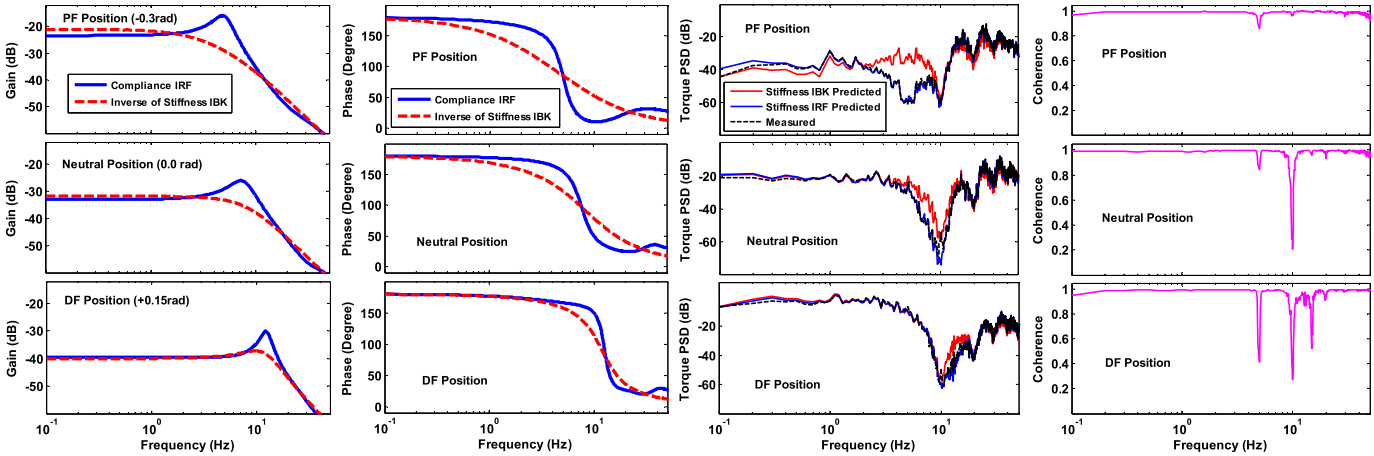

Fig. 4. The gain and phase of the frequency responses of the identified compliance IRFs and the inverse of stiffness IBK of subject S3 at three ankle positions, in addtion to the PSDs of the measured torque and the stiffness IBK and stiffness IRF predicted torques, and the coherences between measured torques and measured position perturbations. Similar results were obtained for the other subjects.

had peaks at corresponding frequencies (see Section B of the Supplementary Material). Torques generated by tremor will appear as noise and so causes the coherence to drop. The effects of tremor on coherence are amplified by the low stiffness of the ankle around 10 Hz, which results in the generation of lower intrinsic torques at this frequency. Note that tremor did not cause deviation from second-order behaviour since the deviation is large at PF position were tremor was absent or extremely small, and it is small at DF position where tremor was large.

Figure 5 presents results that quantify these position dependent changes for all subjects. Fig. 5A shows that the difference between torque prediction VAFs of the stiffness IRF and IBK models, ΔVAF(%), was positive (> 0) for all subjects and at all 7 ankle positions. Thus, the IRF model was always better than the IBK in predicting the ankle torque. In addition, the figure shows that in subjects S1, S2, S3 and S4, the ΔVAF was larger in PF ankle positions than in DF positions. The difference was significant because for subjects S1 to S4 the smallest ΔVAF among all PF positions was larger than the largest ΔVAF among all DF positions. For subject S5, four out of six ΔVAF values at PF positions were larger than four out of six ΔVAF values at DF positions. The statistical significance of this statement was also verified using balanced two-way ANOVA test, where the ankle positions constituted the columns and the subjects corresponded to the rows of the test data matrix (see Section C of the Supplementary Material). As shown in Fig. 5A, the p-value of the two-way ANOVA between columns (or ankle positions) was 3E-20 (with F-statistics of 96.45), which means that the null hypothesis was rejected and thus the results are coming from different distributions. However, the p-values were large when the three PF positions or the two most DF positions were used alone in the test ($p = 0.4980$ and $p = 0.5175$, respectively). Thus, there is no statistical difference among PF positions or among the two most DF positions.

Fig. 5B shows that the fRMSME between the compliance IRF and inverse IBK models, M_{cirf} and $M_{ibk^{-1}}$, increases almost monotonically with ankle plantarflexion. To further emphasize the *static discrepancy* between the two models, we have shown the estimated stiffness IRF gain (or elasticity) K_{irf} as a function of ankle position in Fig. 5C and the difference between the IRF again and the elastic term of the identified IBK model; $\Delta K = K_{irf} - K_{ibk}$, in Fig. 5D. Fig. 5C shows that the elasticity increased significantly as the ankle was dorsiflexed in all subjects. Fig. 5D demonstrates that the IBK model overestimated the elasticity in DF positions larger than 0.05rad and underestimated the elasticity in all PF positions for all subjects.

D. Continuous-Time Compliance Transfer Function Models

We used the multi-step identification procedure of Section II.B to identify continuous-time parametric models of intrinsic ankle compliance at different ankle positions.

1) Compliance Model Order: The IBK model has an a priori fixed order of 2. The IRF model is non-parametric and thus the model order cannot be directly inferred from it. However, transfer function or state-space models can be identified with different model orders. The *order* of a transfer function is equal to the order of its denominator polynomial or the number of its poles. In a state-space model, the order is equal to the dimension of the matrix A of its minimal realization. In **Step-3** of the multi-step identification procedure, we used a subspace method that facilitates compliance model order estimation through singular value decomposition (SVD) of the system's Hankel matrix constructed from input/output data [37]. The model order is the number of dominant singular values.

The subspace method estimated a third-order state-space ankle compliance model for *all* subjects at *all* positions. To further validate this, we manually set the model order in the subspace method to vary from 1 to 6. Fig. 6 shows the impact of model order on normalized sum of squared error (NSSE) of predicting ankle position for all subjects. It is evident that the NSSE decreased monotonically as the model order increased from 1 to 3 and then reached a plateau for models with order 3 and larger. This confirms that the optimal model order is indeed three for all subjects.

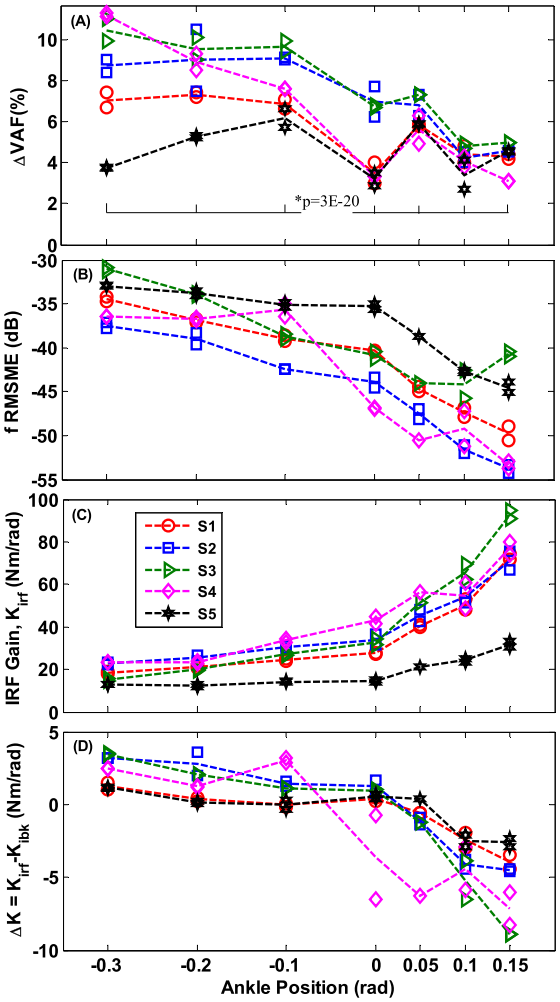

Fig. 5. The ankle position dependency of (A) the difference between torque prediction VAF of the IRF and IBK stiffness models, VAF(%). The asterisks with a p-value of 3E-20 demonstrates that the VAF(%) values come from significantly different distributions based on two-way ANOVA test with p-value threshold of 0.01; (B) the *f*RMSME, in dB, between the compliance IRF and inverse IBK models; (C) the intrinsic elasticity calculated as the stiffness IRF gain; and (D) the difference between the elasticity calculated from the identified stiffness IRF and the elastic term of the IBK model. Note that the results are shown for all subjects at all ankle positions and for all trials (Test and Retest).

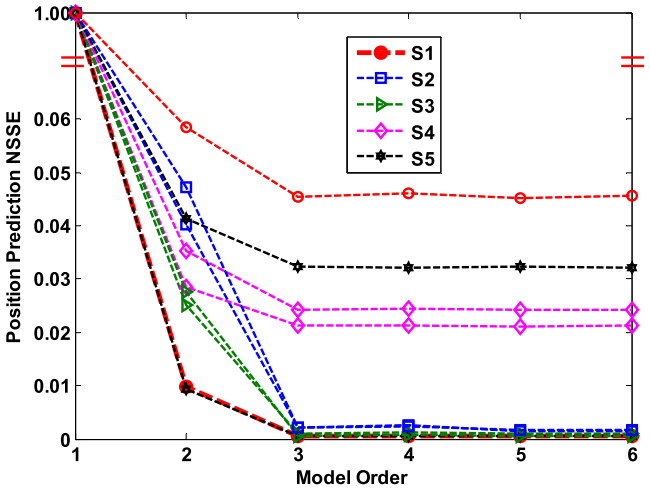

Fig. 6. The impact of the *model order* of the continuous-time transfer function of intrinsic ankle compliance at −0.3rad on normalized SSE of position predictions, using noise-free torque as input, for all subjects and all trials (Test and Retest). Note that the results for subjects S1 and S5 overlay each other.

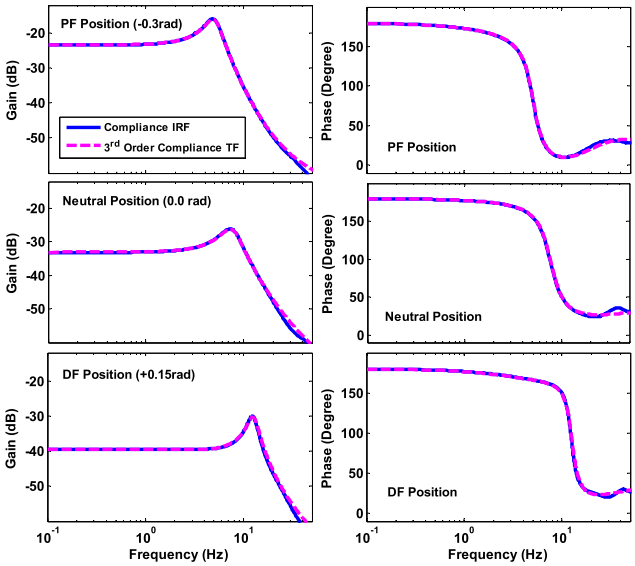

Fig. 7. The gain and phase of the frequency responses of the identified compliance IRFs and the third-order continuous-time compliance TFs of subject S3 at three ankle positions. Similar results were obtained for the other subjects. Note that the gain and phase of the compliance IRFs at different ankle positions are the same as those depicted in Fig. 4.

Figure 7 compares the frequency responses of the compliance IRF (M_{cirf}) and the third-order continuous-time compliance TF (M_{ctf}) models identified at three ankle positions $\{-0.3, 0.0, +0.15\}$rad for a typical subject S3. It is evident from this figure that the third-order TF represented non-parametric compliance IRF gain and phase accurately at all frequencies. Also, comparing Fig. 7 with Fig. 4 reveals that the frequency response of the M_{cirf} is much more similar to the M_{ctf} than the $M_{ibk^{-1}}$. We evaluated this quantitatively at all ankle positions by calculating

$$\Delta fRMSME = \frac{f\text{RMSME}_{M_{cirf},M_{ctf}}}{f\text{RMSME}_{M_{cirf},M_{ibk^{-1}}}}.$$

$\Delta fRMSME$ is a similarity measure for two models *relative to* a reference model (i.e. M_{cirf}) in the frequency domain. In decibels (dB) scale, a negative $\Delta fRMSME$ means that the M_{ctf} is more similar to M_{cirf} than $M_{ibk^{-1}}$. In addition, the more negative this metric, the bigger is the difference between the similarities of the two models to the reference model. Figure 8 shows that $\Delta fRMSME(\text{dB}) \ll 0\text{dB}$, and thus, $f\text{RMSME}_{M_{cirf},M_{ctf}} \ll f\text{RMSME}_{M_{cirf},M_{ibk^{-1}}}$ at all positions for all subjects. This further confirms that the ankle compliance is a third-order system. Note that $\Delta fRMSME(\text{dB})$ is more negative at PF positions since $f\text{RMSME}_{M_{cirf},M_{ibk^{-1}}}$ is larger at PF.

E. Pole/Zero Locations of the Compliance TF

We demonstrated that the ankle compliance TF model is a third-order system. However, the order of a transfer function only determines the number of its poles, while its zeros also have a significant impact on its response. We found that our

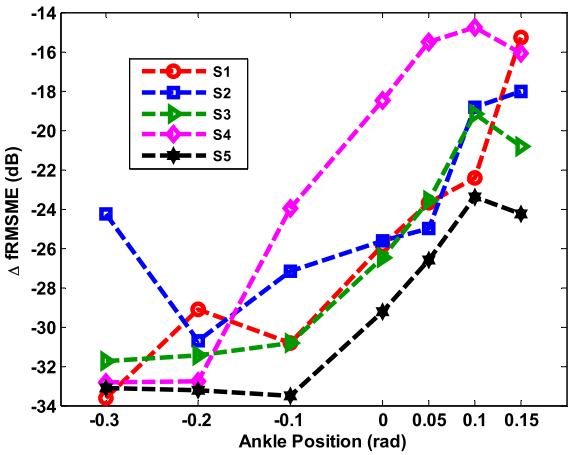

Fig. 8. *ΔfRMSME*, in dB, calculated at all ankle positions for all subjects.

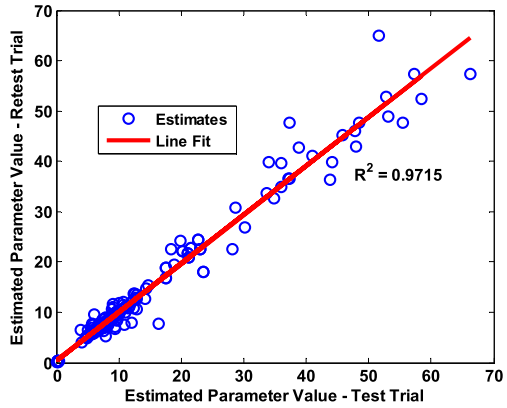

Fig. 9. The scatter plot and the line fit between the parameters of the third-order ankle compliance TF models estimated from Test and Retest trials for all subjects and at all ankle positions.

newly identified continuous-time transfer function model of ankle compliance has two zeros and three poles. They were all negative (or in the left half plane); i.e. poles were stable and zeros were minimum phase. The poles consisted of a real pole and a pair of complex conjugate poles for all subjects at all ankle positions. The two zeros were real at all DF positions for all subjects but complex conjugate in some of the PF and neutral positions (except for S1, where the zeros were real at all positions).

We used a *test-retest* approach to demonstrate that the new ankle compliance model parameters (i.e., poles and zeros), and the multi-step procedure used to identify them, are reliable. For every subject, we performed each trial twice under the same conditions (i.e., same ankle position at rest) and within a short period of time. Then, we applied the multi-step identification procedure to data from each trial, estimated the model parameters, and compared their values. For all subjects, the estimated model parameters were very similar in the two trials. Fig. 9 shows the scatter plot of the estimated parameters from Test and Retest trials for *all* subjects and at *all* ankle positions. These lay along a line with $slope = 0.96$ and an almost zero intercept with $R^2 = 0.97$. The R^2 values of the Test-Retest estimates for each subject were $\{0.99, 0.95, 0.99, 0.97, 0.99\}$, respectively.

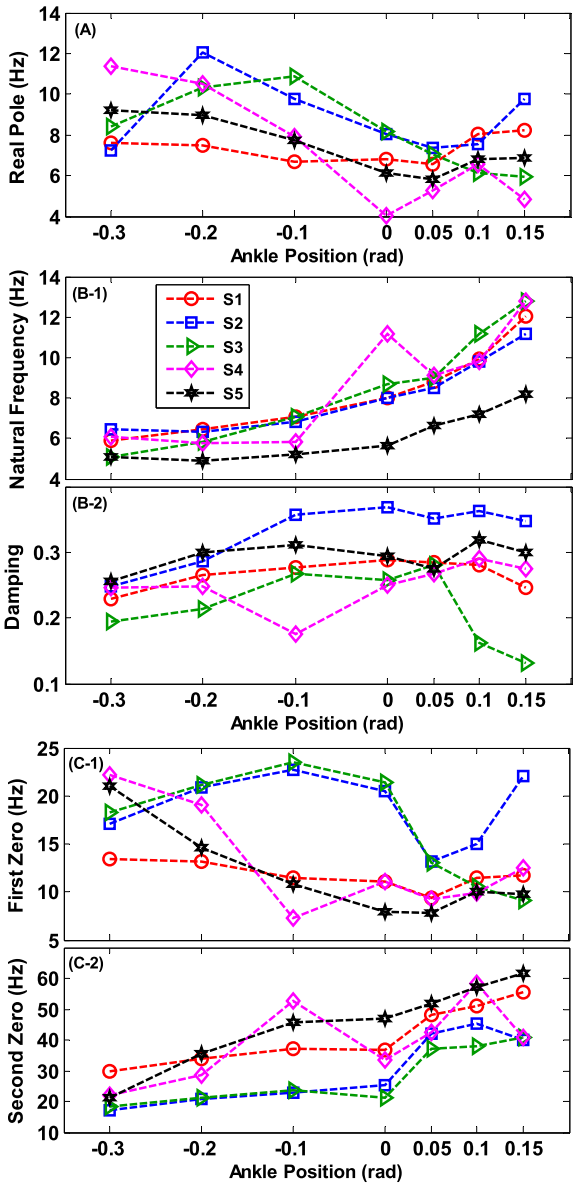

Fig. 10. Changes in the parameters of the identified third-order intrinsic compliance TF with ankle position in five subjects: (A) The real pole, (B-1, B-2) the natural ferquency and damping of the complex conjugate poles, and (C-1,C-2) the two zeros of the TF. The values shown at each position are the average of two estimated values from Test-Retest trials.

F. Effect of Ankle Position on Pole/Zero Locations

We analyzed the changes in the pole/zero locations of the identified ankle compliance TF with joint position to further understand what happens as ankle position changes. The results are shown in Fig. 10 for all subjects. Fig. 10A shows that in all subjects there was no trend in the real pole frequency (in Hz) except that it dropped near neutral (0.0rad) and slightly dorsiflexed ankle positions (0.05rad). However, Fig. 10B-1 shows that the natural frequency of the complex conjugate poles significantly (and almost monotonically) increased with ankle dorsiflexion; it almost doubled from about 5Hz at −0.3rad PF position to about 11Hz at +0.15rad DF position (expect for S3 where it increased to about 8Hz). Fig. 10B-2 shows that the damping coefficients of the complex conjugate poles did not show a consistent trend across the subjects.

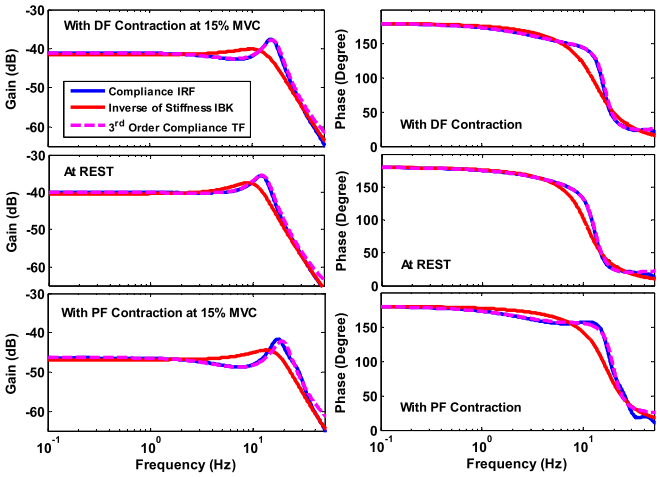

Fig. 11. The gain and phase of the frequency responses of the identified ankle compliance IRF, the third-order continuous-time compliance TF, and the inverse of stiffness IBK of subject S2 at three muscle contraction conditions: 15% MVC DF contraction, REST, and 15% MVC PF contraction. The ankle was at a +0.22rad DF position.

As mentioned earlier, the two zeros of the identified compliance TF were real at all DF positions for all subjects but complex conjugate in some of the PF positions. Nonetheless, the damping coefficients of the complex conjugate zeros were always greater than 0.707 and in most cases very close to 1 (such second-order systems are critically damped and thus do *not* resonate). Hence, those complex conjugate zeros can be approximated with two duplicate real zeros located at their natural frequency. Thus, Fig. 10C-1 shows that one of the zeros did not show a consistent trend with position; it generally became smaller as the ankle was dorsiflexed. Fig. 10C-2 shows that the location of the other zero significantly (and almost) monotonically increased as the ankle was dorsiflexed in all subjects. At +0.15rad DF position, the second real zeros had a frequency well above the expected bandwidth of the ankle compliance. Thus, their effects become negligible and the third-order compliance TFs can be approximated by transfer functions with one zero and three poles at the DF position. In addition, the zero in Fig. 10C-1 and the pole in Fig. 10A became close to each other at +0.15rad DF position causing a near pole-zero cancellation. Such system behaves similarly to a second-order inverse IBK model, which is consistent with the results in Section III.C on the effect of ankle position on the IRF model.

G. What Happens When Ankle Muscles Are Contracted?

We acquired data from subject S2 in two muscle contraction conditions: (1) when he contracted TA muscle at 15% MVC and (2) when he contracted TS muscle group at 15% MVC. The ankle was at a DF position in both conditions. Figure 11 shows the frequency responses of the identified ankle compliance IRFs, third-order compliance TF, and inverse stiffness IBK at the two muscle contraction conditions in addition to the REST condition. It is evident from this figure that the difference between the third-order model and the second-order inverse IBK increases with muscle contraction particularly when TS muscles are active (i.e., muscle contractions that tend to plantarflex the ankle). These preliminary results suggested that the new third-order model is required for accurate modelling of ankle intrinsic mechanics not only at REST condition but also when subjects activate their ankle muscles. The detailed validation of the new model for active ankle is a subject of future work.

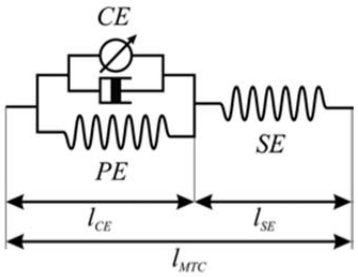

Fig. 12. Schematic of a macroscopic Hill-type muscle model [39].

IV. Discussion

We identified a novel continuous-time, parametric model of intrinsic ankle joint mechanics at rest. The model was identified using a novel multi-step procedure that we developed in this paper. The experimental results from five healthy subjects showed that the passive intrinsic mechanics of the ankle is modelled better by a third-order system than the second-order mass-spring-damper (IBK) model. We observed that the effect of the third-order dynamics is more significant near the PF position of the joint. We also showed that the dynamics of the identified intrinsic compliance are characterized not only by its three poles but also by its two zeros (see Section D of the Supplementary Material). In this section, we will address important questions regarding this new model to (A) understand its underlying (physiological) structure, (B) further confirm its validity, and (C) explore its validity under active muscle conditions.

A. What is the Structure Underlying the Model?

Figure 12 shows the well-known macroscopic Hill-type muscle model [39], where the CE is the contractile element representing the Actin-Myosin interactions, the series-elastic (SE) element represents mainly the *tendons*, the parallel-elastic (PE) element represents muscle elastic tissues such as the deep *fascia* and *sarcolemma* as well as the length-dependent molecular interactions between myosin and actin, and the viscous element in parallel with the CE models the reduction in the muscle force when it is shortening. Note that $CE \cong 0$ when subjects are at REST (i.e. when muscles are *not* contracted).

Figure 13 shows a simple model of muscle organization at the ankle where each muscle is represented by a macroscopic Hill-type model connected to ankle inertia I. The subscript T denotes **T**A muscle and the subscript S denotes T**S** muscle group. The figure shows the three muscles of the TS group {GM, GL, Soleus (Sol.)} with their respective elasticities

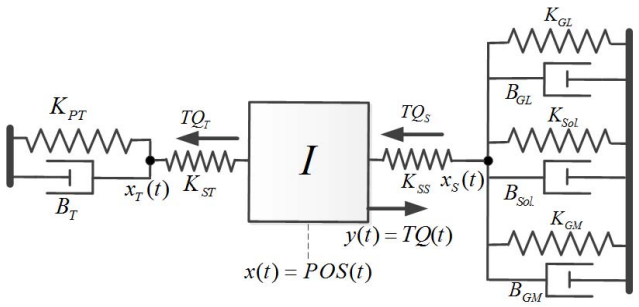

Fig. 13. An structural model of intrinsic ankle biomechanics as an interconnection of Hill-type models of main ankle muscles in *agonist-antagonist* configuration.

$\{K_{GM}, K_{GL}, K_{Sol.}\}$ and viscosities $\{B_{GM}, B_{GL}, B_{Sol.}\}$. However, since these three muscles are connected in parallel to ankle via a single tendon - *calcaneus* tendon - and the knee is fixed in our experimental setup, their elastic and viscous properties simply add. Thus, the elasticity K_{PS} and damping B_S of the equivalent TS model is

$$\begin{aligned} K_{PS} &= K_{GM} + K_{GL} + K_{Sol.} \\ B_S &= B_{GM} + B_{GL} + B_{Sol.} \end{aligned} \tag{9}$$

Considering the equivalent TS model, we obtained the compliance transfer function of the model structure shown in Fig. 13 (see Appendix for details)

$$H_{compl.}(s) = \frac{X(s)}{Y(s)} = H^{-1}_{stiff}(s) = \frac{b_2 s^2 + b_1 s + b_0}{a_3 s^3 + a_2 s^2 + a_1 s + a_0} \tag{10}$$

where

$$\begin{aligned} b_2 &= B_T B_S \\ b_1 &= B_S \sigma_T + B_T \sigma_S \\ b_0 &= \sigma_T \cdot \sigma_S \\ a_3 &= I\,(B_T + B_S) \\ a_2 &= I\,(\sigma_T + \sigma_S) + B_T B_S\,(K_{SS} + K_{ST}) \\ a_1 &= B_T K_{ST} \sigma_S + B_S K_{SS} \sigma_T + B_T \Delta_S + B_S \Delta_T \\ a_0 &= \Delta_T \sigma_S + \Delta_S \sigma_T . \end{aligned}$$

The compliance TF in (10) has two zeros, three poles and seven parameters $[\mathrm{I}, \mathrm{B_T}, \mathrm{K_{PT}}, \mathrm{K_{ST}}, \mathrm{B_S}, \mathrm{K_{PS}}, \mathrm{K_{SS}}]$, or more precisely, 11 parameters considering (9). The new parametric model identified from experimental data using the multi-step procedure also had two zeros and three poles. Therefore, the structural model proposed for ankle in Fig. 13 is consistent with the third-order ankle compliance TF model identified from experimental data.

We also analyzed the behavior of the model structure shown in Fig. 13 as the ankle is dorsiflexed. At an extreme DF position, the TA muscle is shortened while all TS muscles are extended. Therefore, the TS group acts like a much stronger spring than the TA; i.e., $K_{PS} \gg K_{PT}$ and $K_{SS} \gg K_{ST}$. This means that the TA Hill-type model on the left side of ankle inertia in Fig. 13 can be neglected. With only the equivalent model of TS group attached to the right side of the ankle inertia in Fig. 13 the compliance transfer function becomes:

$$H_{compl.}(s) \cong \frac{B_S s + (K_{PS} + K_{SS})}{I.B_S s^3 + I\,(K_{PS} + K_{SS})\,s^2 + B_S K_{SS} s + K_{PS}.K_{SS}}. \tag{11}$$

This compliance transfer function has one real zero and three poles (two complex conjugate and a real). This is consistent with the observations made from the experimental analysis of the ankle dorsiflexion effect on pole-zero locations in Section III.F. Hence, the compliance transfer function of the *structural model* also approaches a second-order inverse IBK as the ankle is dorsiflexed.

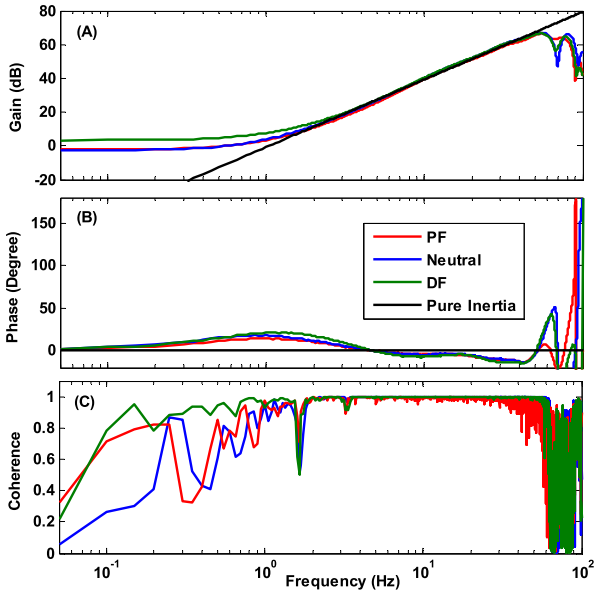

Fig. 14. The frequency responses of the identified stiffness IRFs of the *calibration load* at three different positions (PF, Neutral, DF) are very similar to that of a pure inertial load in the [2,50]Hz frequency range: (A) the gain, (B) the phase, and (C) the coherence between position and torque.

B. Why is it Not the Boot or Foot/Boot Interface?

One hypothesis is that the dynamics not modelled by the IBK and captured by the third-order model are associated with the boot or the foot/boot interface. We ruled out this hypothesis both experimentally and theoretically. First, we performed a calibration experiment where we used a *calibration load* made of an aluminum bar whose shape and inertia were similar to a typical foot and wrapped it in a custom built boot. Then, we placed the load into our hydraulic system and repeated the small signal perturbation experiments at PF, Neutral and DF positions. The gain of the frequency response of the identified stiffness IRF shown in Fig. 14A indicates that the calibration load was a *pure inertia* and *no* unexpected dynamics (i.e., that is not part of the inertial load) were identified. The phase shown in Fig. 14B also resembles that of an inertial load since it is almost constant and near zero up to almost 60 Hz, where coherence is large. Note in Fig. 14C that the coherence between position and torque drops at low frequencies where

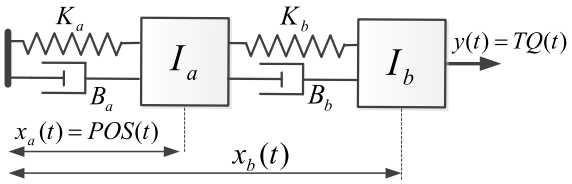

Fig. 15. An structural model consisting of a series interconnection of IBK models for ankle and the boot.

there is little output power. Also note that the identified system is almost the same at all positions. In conclusion, we believe that the dynamics identified by the IRF and TF models for the ankle cannot be explained by the boot or boot/foot interface.

Then, we demonstrated theoretically that the new third-order dynamics is not associated with the boot or the foot/boot interface. Consider the model structure shown in Fig. 15, where ankle mechanics is represented by a conventional IBK model and the foot/boot interface is modeled by another IBK in series with it, similar to de Vlugt *et al.* [13]. It can be shown that the compliance transfer function of this model structure has a single zero and four poles

$$H_{compl.}(s)\frac{X_a(s)}{Y(s)} = \frac{B_b s + K_b}{(I_a + I_b)s^4 + a_3 s^3 + a_2 s^2 + a_1 s + K_a K_b} \tag{12}$$

where I_b, B_b, K_b and I_a, B_a, K_a are the inertia, viscosities and elasticities of the boot and ankle, respectively; $a_3 = I_a B_b + I_b (B_a + B_b)$; $a_2 = K_b (I_a + I_b) + K_a I_b + B_a B_b$; and $a_1 = K_a (B_a + B_b)$. Thus, this model is *not* consistent with the model identified from experimental data.

C. The Significance of the New third-order Model

The results of this paper are important because they revealed that passive ankle joint dynamics cannot be fully described by second-order IBK models. More specifically, we could not fit *both* low-frequency and resonance dynamics with IBK model and had to trade-off one for another. We showed that a second-order model is not adequate in the frequency ranges of 0.5-15 Hz when the ankle is plantarflexed and 5-15Hz when the ankle is in Neutral position. However, the third-order model with 2 zeros and 3 poles does represent joint stiffness well at all frequencies including low frequencies and resonant frequency. Even though deviations from second-order IBK model was reported by, for example, Lee *et al.* [4], the dynamic nature and physiological interpretations of these deviations were not identified and systematically investigated in the literature. However, our comprehensive experimental identification studies and analytical studies with Hill-type muscle models suggested that the dynamics associated with distinct physiological elements of the joint such as tendons (SE) and muscle elastic tissues like deep fascia and sarcolemma (PE) can be represented and separated *only* by a third-order model. In addition, a third-order model with two zeros (as opposed to the inverse IBK model with no zeros) is required to capture the true response of the agonist-antagonist muscles acting simultaneously on the joint. Finally, the newly identified third-order model is necessary to accurately predict intrinsic ankle torque in response to wide band inputs or position perturbations. As such, joint stiffness identification studies that use the parametric IBK model structure would not always be accurate. Consequently, non-parametric IRF model or higher order parametric models like the identified third-order model should be used.

D. Limitations of the Study

This study identified a new parametric model of ankle joint dynamic stiffness that was supported by a biologically-motivated physical mechanism based on ankle physiology and the Hill-type muscle model. Even though such a model contributes to our understanding of human neuro-muscular biomechanics, the extent to which it can be generalized to activities of daily living (ADL) must be studied and investigated. This study was done in relaxed (or passive) and supine (fixed knee angle) conditions that are not prevalent in many ADL such as walking and upright stance, where:

- The knee angle changes, which will modulate ankle stiffness due to changes it creates in TS muscle length.
- Muscle activation changes, which will modulate the ankle stiffness parameters. In such cases, we have to use time-varying or linear parameter varying (LPV) representations to model stiffness (e.g., Sobhani Tehrani *et al.* [25]).

In addition, this study focused on situations where reflex responses were mostly absent or very small (in 1 subject). However, reflexes exist in some ADL and in fact change depending on the context of the motor task performed. The validity of the third-order model in presence of significant reflexes should be investigated.

Finally, this study focused on only the ankle joint. The extent to which the third-order model applies to other joints having different agonist-antagonist muscle pair structures is an interesting and compelling topic of future work. For example, in the knee joint, multiple muscles act on the joint through different tendons. A detailed analysis of the knee anatomy will be required to assess the validity of the third-order model for it.

APPENDIX

To obtain the compliance transfer function of the model structure shown in Fig. 11, we first applied Newton's second law of motion to ankle joint

$$y - K_{ST}(x - x_T) - K_{SS}(x - x_S) = I\ddot{x} \tag{13}$$

where I is the inertia of the ankle/foot; $x(t) = POS(t)$ is ankle position and $y(t) = TQ(t)$ is the torque acting about it; K_{ST} and K_{SS} are the series elastic elements of **T**A and equivalent T **S** models representing TA and *calcaneal* tendons; and $x_T(t)$ and $x_S(t)$ are the positions of the connection points of TA and TS muscles to their tendons.

The spring and damper forces of the model in Fig. 11 are related together

$$\begin{aligned} K_{ST}(x - x_T) &= K_{PT}x_T + B_T\dot{x}_T \\ K_{SS}(x - x_S) &= K_{PS}x_S + B_S\dot{x}_S \end{aligned} \tag{14}$$

where K_{PS} and B_S were defined in (9), and K_{PT} is the PE and B_T is the viscosity of the TA muscle. Writing (14) in Laplace domain, we can relate $X_T(s)$ and $X_S(s)$ to $X(s)$

$$X_T(s) = \frac{K_{ST}}{B_T s + (K_{PT} + K_{ST})} X(s)$$
$$X_S(s) = \frac{K_{SS}}{B_S s + (K_{PS} + K_{SS})} X(s) \tag{15}$$

Inserting (15) in the Laplace domain representation of (13), we obtain the stiffness transfer function of the model in Fig. 11

$$H_{stiff}(s) \frac{Y(s)}{X(s)} = Is^2 + \frac{B_T K_{ST} s + \Delta_T}{B_T s + \sigma_T} + \frac{B_S K_{SS} s + \Delta_S}{B_S s + \sigma_S} \tag{16}$$

where

$$\Delta_T \triangleq K_{PT} \cdot K_{ST}; \quad \sigma_T \triangleq K_{PT} + K_{ST}$$
$$\Delta_S \triangleq K_{PS} \cdot K_{SS}; \quad \sigma_S \triangleq K_{PS} + K_{SS}.$$

Combining the terms and inverting the stiffness transfer function, we obtain the compliance transfer function in (10).

REFERENCES

[1] R. E. Kearney, R. B. Stein, and L. Parameswaran, "Identification of intrinsic and reflex contributions to human ankle stiffness dynamics," *IEEE Trans. Biomed. Eng.*, vol. 44, no. 6, pp. 493–504, Jun. 1997.

[2] E. J. Rouse, L. J. Hargrove, E. J. Perreault, and T. A. Kuiken, "Estimation of human ankle impedance during the stance phase of walking," *IEEE Trans. Neural Syst. Rehabil. Eng.*, vol. 22, no. 4, pp. 870–878, Jul. 2014.

[3] G. L. Gottlieb and G. C. Agarwal, "Dependence of human ankle compliance on joint angle," *J. Biomech.*, vol. 11, no. 4, pp. 177–181, 1978.

[4] H. Lee, P. Ho, M. Rastgaar, H. I. Krebs, and N. Hogan, "Multivariable static ankle mechanical impedance with active muscles," *IEEE Trans. Neural Syst. Rehabil. Eng.*, vol. 22, no. 1, pp. 44–52, Jan. 2014.

[5] P. L. Weiss, R. E. Kearney, and I. W. Hunter, "Position dependence of ankle joint dynamics—II. Active mechanics," *J. Biomech.*, vol. 19, no. 9, pp. 737–751, 1986.

[6] H. Lee, P. Ho, M. A. Rastgaar, H. I. Krebs, and N. Hogan, "Multivariable static ankle mechanical impedance with relaxed muscles," *J. Biomech.*, vol. 44, pp. 1901–1908, Jul. 2011.

[7] P. L. Weiss, R. E. Kearney, and I. W. Hunter, "Position dependence of ankle joint dynamics—I. Passive mechanics," *J. Biomech.*, vol. 19, no. 9, pp. 727–735, 1986.

[8] K. Kubo, D. Miyazaki, K. Yamada, H. Yata, S. Shimoju, and N. Tsunoda, "Passive and active muscle stiffness in plantar flexors of long distance runners," *J. Biomech.*, vol. 48, no. 10, pp. 1937–1943, 2015.

[9] D. A. Winter, A. E. Patla, S. Rietdyk, and M. G. Ishac, "Ankle muscle stiffness in the control of balance during quiet standing," *J. Neurophysiol.*, vol. 85, no. 6, pp. 2630–2633, 2001.

[10] E. J. Rouse, R. D. Gregg, L. J. Hargrove, and J. W. Sensinger, "The difference between stiffness and quasi-stiffness in the context of biomechanical modeling," *IEEE Trans. Biomed. Eng.*, vol. 60, no. 2, pp. 562–568, Feb. 2013.

[11] D. L. Morgan, "Separation of active and passive components of short-range stiffness of muscle," *Amer. J. Physiol.-Cell Physiol.*, vol. 232, no. 1, pp. 45–49, 1977.

[12] M. Vlutters, T. A. Boonstra, A. C. Schouten, and H. van der Kooij, "Direct measurement of the intrinsic ankle stiffness during standing," *J. Biomech.*, vol. 48, no. 7, pp. 1258–1263, 2015.

[13] E. de Vlugt, S. van Eesbeek, P. Baines, J. Hilte, C. G. M. Meskers, and J. H. de Groot, "Short range stiffness elastic limit depends on joint velocity," *J. Biomech.*, vol. 44, no. 11, pp. 2106–2112, 2011.

[14] S. van Eesbeek, J. H. de Groot, F. C. T. van der Helm, and E. de Vlugt, "*In vivo* estimation of the short-range stiffness of cross-bridges from joint rotation," *J. Biomech.*, vol. 43, pp. 2539–2547, Sep. 2010.

[15] E. Burdet, R. Osu, D. W. Franklin, T. Yoshioka, T. E. Milner, and M. Kawato, "A method for measuring endpoint stiffness during multi-joint arm movements," *J. Biomech.*, vol. 33, no. 12, pp. 1705–1709, Dec. 2000.

[16] E. J. Perreault, R. F. Kirsch, and P. E. Crago, "Voluntary control of static endpoint stiffness during force regulation tasks," *J. Neurophysiol.*, vol. 87, no. 6, pp. 2808–2816, Jun. 2002.

[17] R. E. Kearney and I. W. Hunter, "System identification of human joint dynamics," *Critical Rev. Biomed. Eng.*, vol. 18, no. 1, pp. 55–87, 1990.

[18] E. J. Perreault, R. F. Kirsch, and A. M. Acosta, "Multiple-input, multiple-output system identification for characterization of limb stiffness dynamics," *Biol. Cybern.*, vol. 80, pp. 327–337, May 1999.

[19] D. T. Westwick and R. E. Kearney, "Identification of physiological systems: A robust method for non-parametric impulse response estimation," *Med. Biol. Eng. Comput.*, vol. 35, pp. 83–90, Mar. 1997.

[20] D. T. Westwick and E. J. Perreault, "Estimates of acausal joint impedance models," *IEEE Trans. Biomed. Eng.*, vol. 59, no. 10, pp. 2913–2921, Oct. 2012.

[21] E. J. Perreault, P. E. Crago, and R. F. Kirsch, "Estimation of intrinsic and reflex contributions to muscle dynamics: A modeling study," *IEEE Trans. Biomed. Eng.*, vol. 47, no. 11, pp. 1413–1421, Nov. 2000.

[22] H. Lee and N. Hogan, "Time-varying ankle mechanical impedance during human locomotion," *IEEE Trans. Neural Syst. Rehabil. Eng.*, vol. 23, no. 5, pp. 755–764, Sep. 2015.

[23] M. M. Mirbagheri, H. Barbeau, and R. E. Kearney, "Intrinsic and reflex contributions to human ankle stiffness: Variation with activation level and position," *Experim. Brain Res.*, vol. 135, pp. 423–436, Dec. 2000.

[24] S. Pfeifer, H. Vallery, M. Hardegger, R. Riener, and E. J. Perreault, "Model-based estimation of knee stiffness," *IEEE Trans. Biomed. Eng.*, vol. 59, no. 9, pp. 2604–2612, Sep. 2012.

[25] E. S. Tehrani, K. Jalaleddini, and R. E. Kearney, "Linear parameter varying identification of ankle joint intrinsic stiffness during imposed walking movements," in *Proc. 35th IEEE EMBS Conf.*, Jul. 2013, pp. 4923–4927.

[26] M. Sartori, M. Maculan, C. Pizzolato, M. Reggiani, and D. Farina, "Modeling and simulating the neuromuscular mechanisms regulating ankle and knee joint stiffness during human locomotion," *J. Neurophysiol.*, v. 114, no. 4, pp. 2509–2527, 2015.

[27] D. J. Bennett, J. M. Hollerbach, Y. Xu, and I. W. Hunter, "Time-varying stiffness of human elbow joint during cyclic voluntary movement," *Experim. Brain Res.*, vol. 88, pp. 433–442, Feb. 1992.

[28] M. A. Krutky, R. D. Trumbower, and E. J. Perreault, "Influence of environmental stability on the regulation of end-point impedance during the maintenance of arm posture," *J. Neurophysiol.*, vol. 109, pp. 1045–1054, Feb. 2013.

[29] M. S. Erden and A. Billard, "End-point impedance measurements across dominant and nondominant hands and robotic assistance with directional damping," *IEEE Trans. Cybern.*, vol. 45, no. 6, pp. 1146–1157, Jun. 2015.

[30] M. Ditroilo, L. Cully, C. A. G. Boreham, and G. De Vito, "Assessment of musculo-articular and muscle stiffness in young and older men," *Muscle Nerve*, vol. 46, no. 4, pp. 559–565, 2012.

[31] R. B. Stein and R. E. Kearney, "Nonlinear behavior of muscle reflexes at the human ankle joint," *J. Neurophysiol.*, vol. 73, no. 1, pp. 65–72, Jan. 1995.

[32] K. Jalaleddini, E. S. Tehrani, and R. Kearney, "A subspace approach to the structural decomposition and identification of ankle joint dynamic stiffness," *IEEE Trans. Biomed. Eng.*, to be published, doi: 10.1109/TBME.2016.2604293.

[33] R. E. Kearney and I. W. Hunter, "Dynamics of human ankle stiffness: Variation with displacement amplitude," *J. Biomech.*, vol. 15, no. 10, pp. 753–756, 1982.

[34] M. Verhaegen and V. Verdult, *Filtering and System Identification: A Least Squares Approach*. Cambridge, U.K.: Cambridge Univ. Press, 2007.

[35] L. Ljung, *System Identification: Theory for the User*, 2nd ed. Upper Saddle River, NJ, USA: Prentice-Hall, 1999.

[36] M. Verhaegen and P. Dewilde, "Subspace model identification part 1. The output-error state-space model identification class of algorithms," *Int. J. Control*, vol. 56, pp. 1187–1210, Nov. 1992.

[37] B. Haverkamp, C. T. Chou, and M. Verhaegen, "SMI toolbox: A MATLAB toolbox for state space model identification," *J. A*, vol. 38, no. 3, pp. 34–37, 1997.

[38] K. Jalaleddini and R. E. Kearney, "Subspace method decomposition and identification of the parallel-cascade model of ankle joint stiffness: Theory and simulation," in *Proc. 35th IEEE EMBS Conf.*, Jul. 2013, pp. 5071–5074.
[39] P. Gribble. (Jun. 2014). *Lecture Notes on Computational Modeling in Neuroscience*. [Online]. Available: http://gribblelab.org/compneuro/index.html

Ehsan Sobhani Tehrani (S'13–M'17) received the B.Sc. degree in electrical engineering from Amirkabir University of Technology, Tehran, Iran, in 2003, and the M.A.Sc. degree in electrical and computer engineering from Concordia University, Montréal, Canada, in 2008. He is currently pursuing the Ph.D. degree with the Department of Biomedical Engineering, McGill University, Montréal. He is also a Senior Systems Engineer and the Chief Technology Officer of GlobVision Inc., Saint-Laurent, QC, Canada. His areas of expertise are in human biomechanics and motor control, system identification, physiological signal processing, estimation, filtering and prediction, fault diagnosis, computational intelligence and machine learning, and modeling and simulation of dynamical systems (physiological and engineering).

Kian Jalaleddini (S'08–M'16) received the B.Sc. in electrical engineering from the University of Tehran, Tehran, Iran, in 2007, the M.A.Sc. degree in electrical and computer engineering from Concordia University, Montréal, Canada, in 2009, and the Ph.D. degree in biomedical engineering from McGill University, Montréal, Canada, in 2015. He is currently a Post-Doctoral Scholar with the Division of Biokinesiology and Physical Therapy, University of Southern California.

His research interests include analysis of biomedical signals and systems, development and application of system identification tools, exploring biomechanics of human joints and spinal reflexes.

Prof. Jalaleddini has served as the Chair of the IEEE Engineering in Medicine and Biology Chapter, Montréal Section from 2011 to 2015, and a Secretary of the IEEE Montréal Section from 2010 to 2013.

Robert E. Kearney (M'76–SM'92–LM'01–LF'13) received the undergraduate, Master's, and Ph.D. degrees from McGill University in 1968, 1971, and 1976, respectively, all in mechanical engineering.

He is currently a Professor and the Chair of the Department of Biomedical Engineering with the Faculty of Medicine, McGill University. He maintains an active research program that focuses on using quantitative engineering techniques to address important biomedical problems. His research interests include the development of algorithms and tools for biomedical system identification, the application of system identification to understand the role played by peripheral mechanisms in the control of posture and movement, and the development of signal processing and machine learning methods for respiratory monitoring. His research is supported by NSERC, CIHR, and the Qatar National Research Fund.

Dr. Kearney is a Professional Engineer, a fellow of the Engineering Institute of Canada, and the American Institute of Medical and Biological Engineering.